Boundary Layer Controls on Shallow Cumulus Convection at ARM-SGP

Neil P. Lareau[1], Yunyan Zhang[2] and Stephen A. Klein[2]

[1]Department of Meteorology and Climate Science, San José State University, [2]Lawrence Livermore National Laboratory

1. Introduction

Shallow cumulus (ShCu) are an important component of the climate system, impacting both the surface energy budget and boundary layer development. Despite their importance, ShCu remain poorly represented in global climate models due to their sub-grid-scale size (~ 1 km) and uncertainties in their relationship to resolved-scale variables. With this in mind, the goals of this study are:
1. Improve our understanding cloud-layer–boundary-layer interactions on ShCu days.
2. Test the applicability of the CIN-based mass flux closure for continental ShCu using observations.

This study uses a suite of observations from ARM-SGP including: Doppler Lidar, Raman Lidar, Microwave radiometer profiler, Balloon-borne soundings, Atmospheric emitted radiance interferometer (AERI) profiles, surface flux observations (ECOR), and other near surface meteorological data. Using these data we examine the mean CBL and cloud layer properties on ShCu days as well as the relationship amongst vertical velocity in the sub-cloud layer, stratification in the cloud layer, and cloud properties.

Event Identification: ShCu days are selected using the following criteria:
(1) Qualitative assessment of ShCu development from visible satellite data to ensure local forcing characteristics.
(2) A well-developed convective boundary layer (CBL), determined from the Doppler lidar observations.
(3) Clouds bases closely coupled to the CBL evolution, as determined from the lidar observations.
(4) Minimal mid and upper level cloudiness.
(5) No precipitation
Using these criteria a total of 138 ShCu days are selected from the warm season (Apr.-Sept.) 2011-2015.
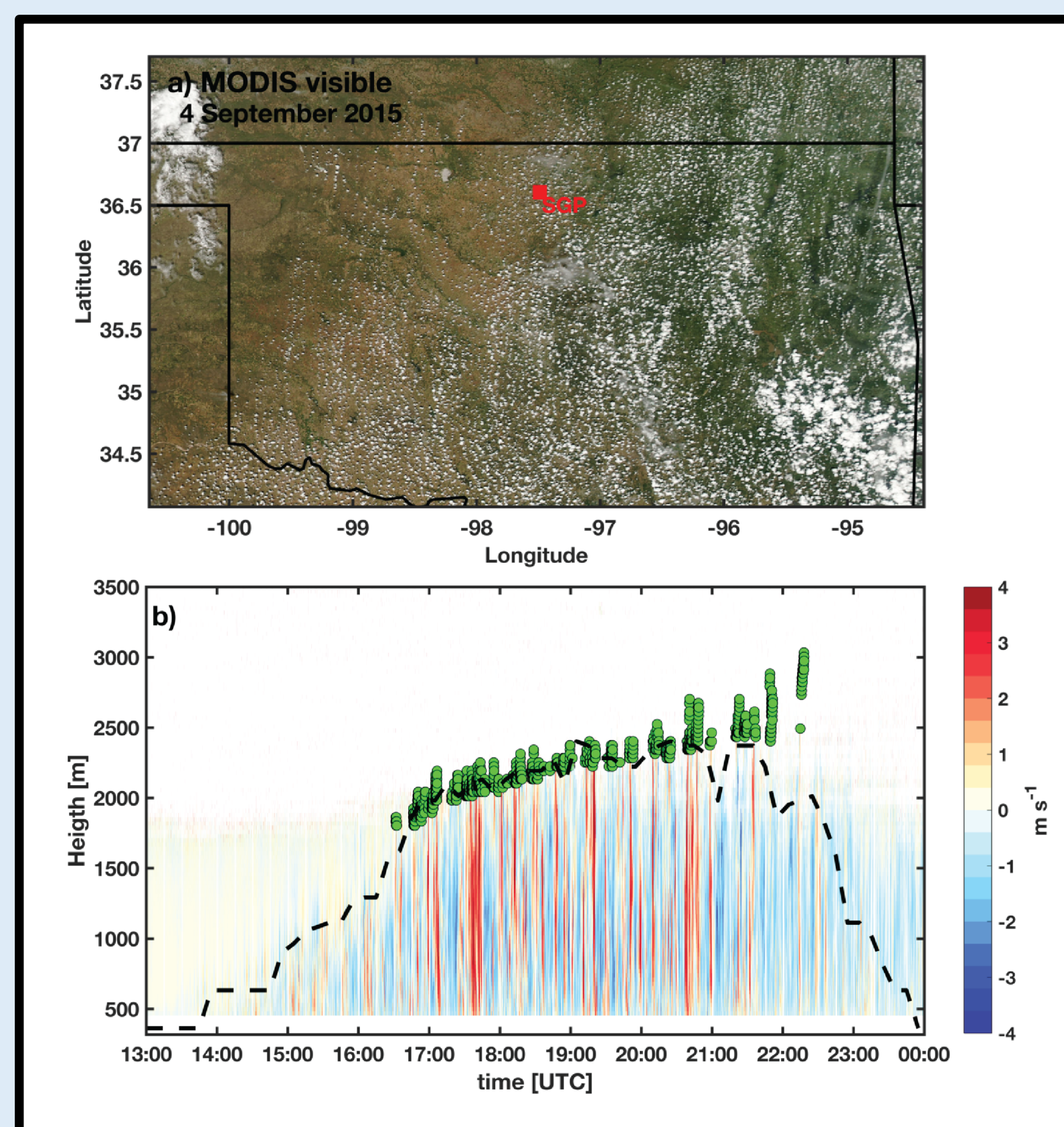
Fig. 1 Example of a shallow cumulus on 4 September 2015 at ARM-SGP. (a) MODIS-AQUA visible imagery showing the distribution of locally forced convective clouds (b) Doppler lidar observations from 4 September 2015 showing the vertical velocity (color shading), derived convective boundary layer height (dashed black line), and cloud base detections (green dots).

2. The ShCu Boundary Layer

Figure 2 shows the composite CBL on ShCu days using data from the Doppler lidar. The composite shows the vertical velocity (VV) variance (gray shading), VV skewness (red contours), cloud base heights (circles), cloud fraction (color fill on circles), lifting condensation level (LCL, green dashed line), and the derived CBL height (black line). The VV variance is proportional to the turbulence kinetic energy. The VV skewness is strongly positive throughout, indicative of narrow updrafts flanked by broader downdrafts.

Cloud initiation occurs at 1725 UTC (1125 CST), corresponding to the intersection of the CBL top with the LCL. Following initiation, the cloud base height remains closely coupled to the CBL top until ~2100 UTC, after which clouds decouple from the boundary layer turbulence. Cloud fraction peaks at 23%.

The corresponding potential temperature and Brunt-Vaisala frequency are shown in Fig. 3. These data show a nocturnal inversion that gives way to near neutral stratification within the growing CBL. The CBL top is characterized by stronger stratification with a maximum in N aloft in the afternoon (red contours for emphasis).

The composite boundary layer relative humidity (RH) and mixing ratio, determined from the Raman Lidar, is shown in Fig. 4. The RH increases along the top edge of the CBL, reaching a maximum at the time of maximum cloud fraction. High mixing ratio air is mixed upward in the growing CBL during this time. Notable the vertical gradient in mixing ratio increasing significantly in the afternoon (dashed contours)
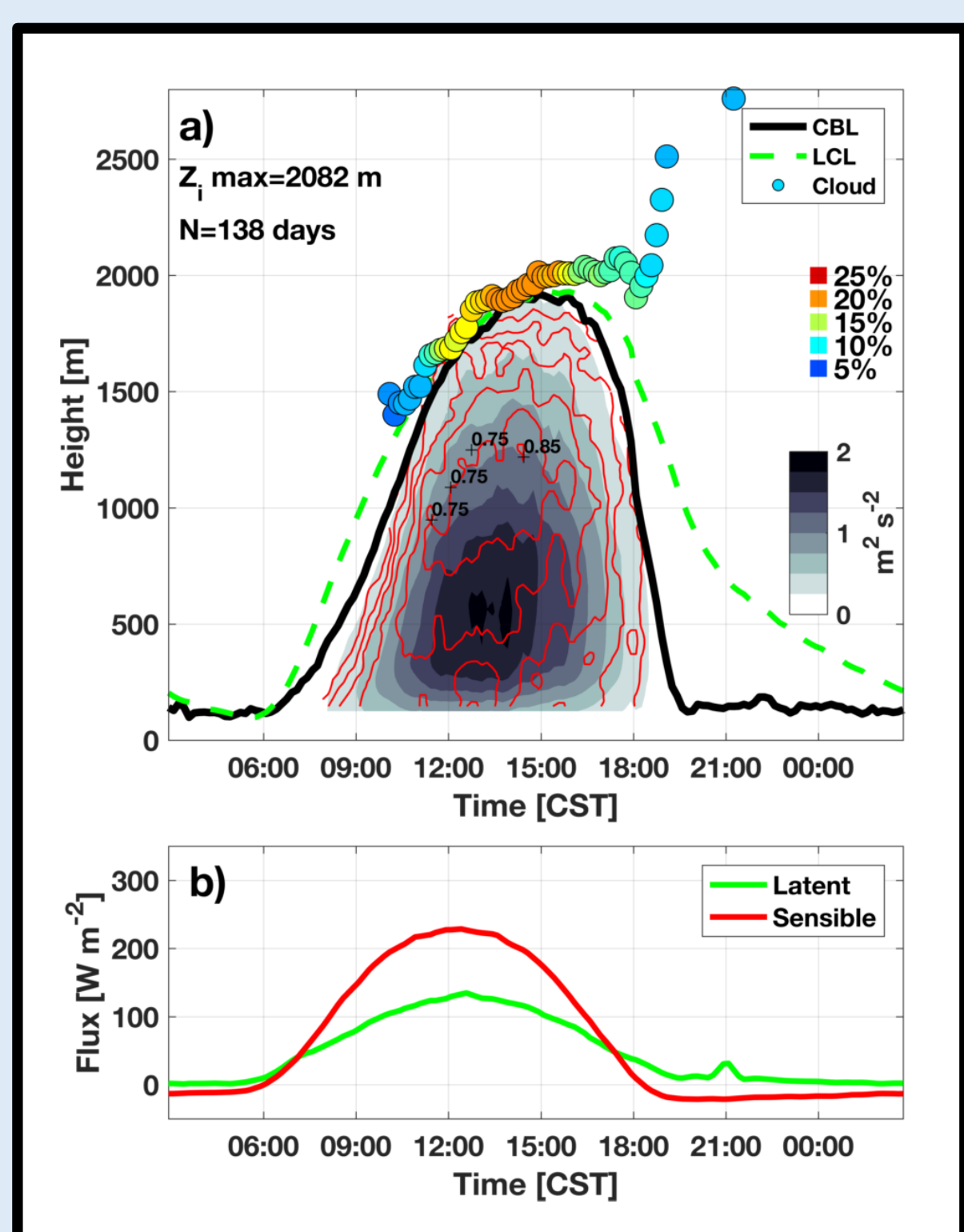
Figure 2 Composite CBL evolution and surface forcing on ShCu days. See text for explanation.
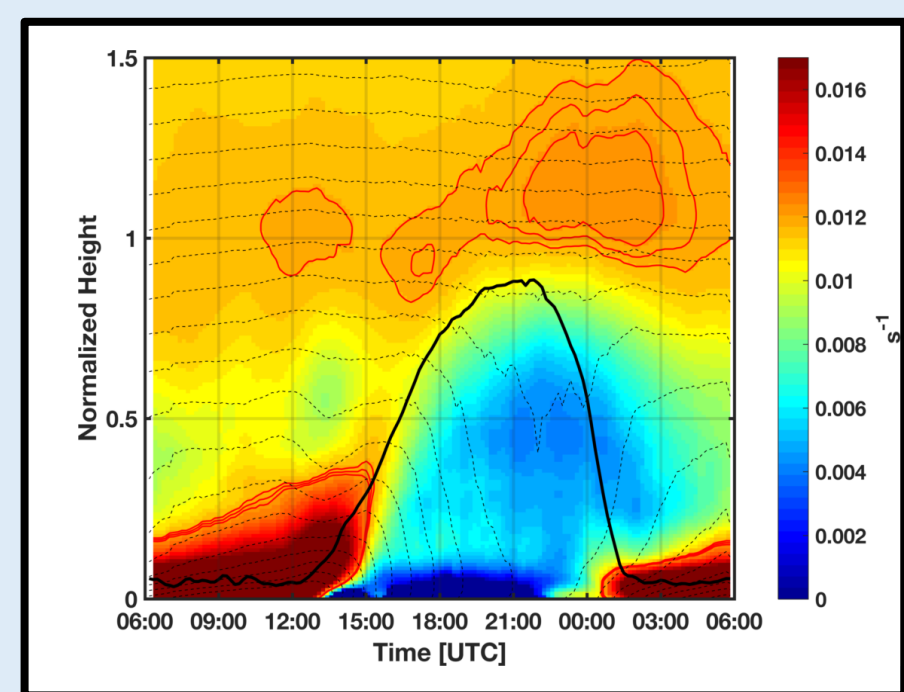
Fig. 3. Composite Brunt-Vaisala frequency (shaded) and potential temperature (dashed contours, c.i. 1 K) from the AERI profiler. The CBL height is shown as a solid black line.. Heights are normalized by the CBL height.

Fig. 4. Composite analysis of CBL humidity from the Raman Lidar. (a) CBL relative humidity. (b) CBL mixing ratio (shaded) and the vertical gradient of the mixing ratio (dashed contours). The dashed black line is the mean CBL height.
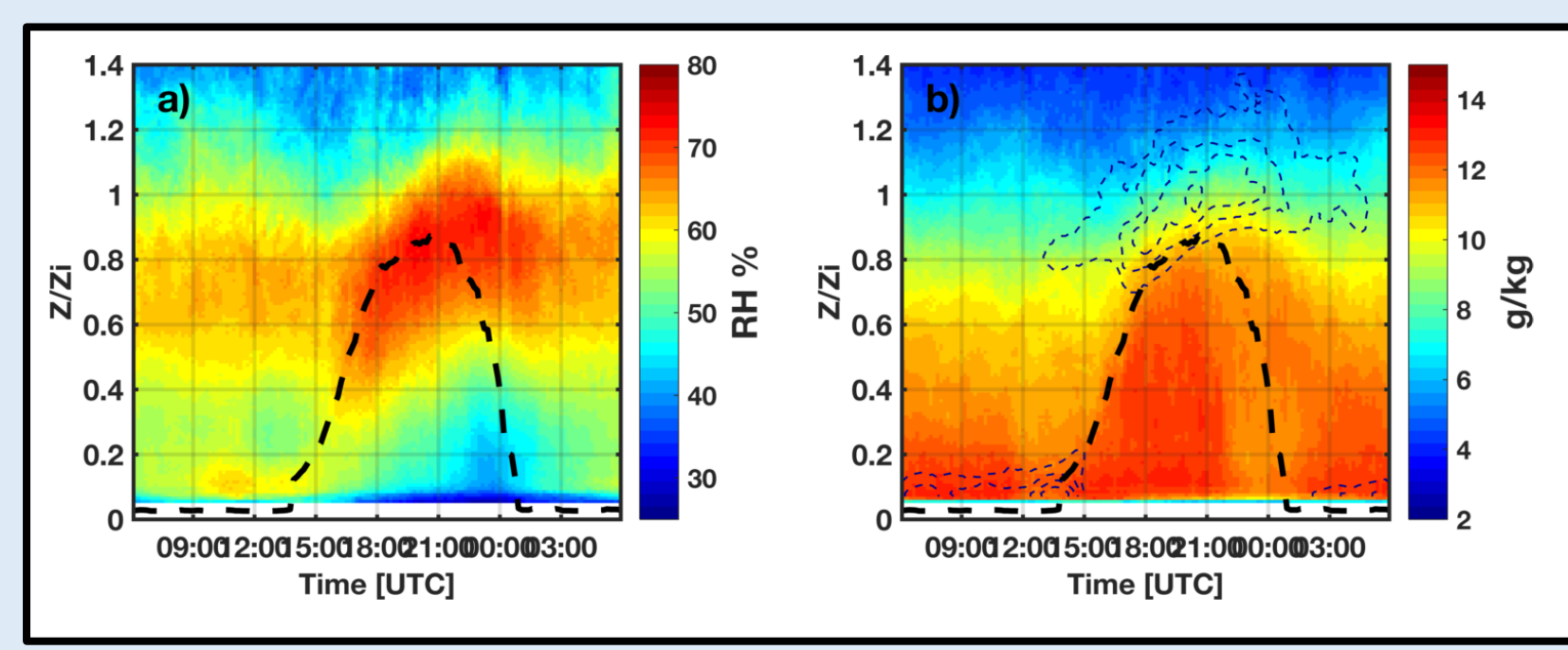
3. Individual Cloud Statistics

Individual clouds are defined as temporally continuous vertical scans with backscatter above an empirical threshold. The cloud identification also requires cloud base to be within 200 m of the CBL top and cloud duration less than 20 minutes. Short gaps in cloud returns are permitted. An example cloud identification is shown in Fig. 5a, b.

Once identified, each cloud is characterized by its duration, chord length, LWP, cloud base updrafts, and cloud base mass flux. The cloud base mass flux is computed as:

$$M_{cb} = \rho[\sigma_u W_u + \sigma_d W_d]$$

where σ_u, σ_d are the updraft and downdraft fractions for a given cloud and W_u and W_d are the mean updraft/downdraft speeds. We also extract a subcloud vertical velocity "scene" associated with each cloud. The time and height of these scenes are normalized by cloud base height and cloud duration, respectively (Fig. Xc)

In total 1495 clouds are identified. The cloud base mass flux distribution for these clouds indicates that 63% of clouds are characterized by a net positive mass flux, implying an upward redistribution of mass from the CBL into the cloud layer (Fig. 6)
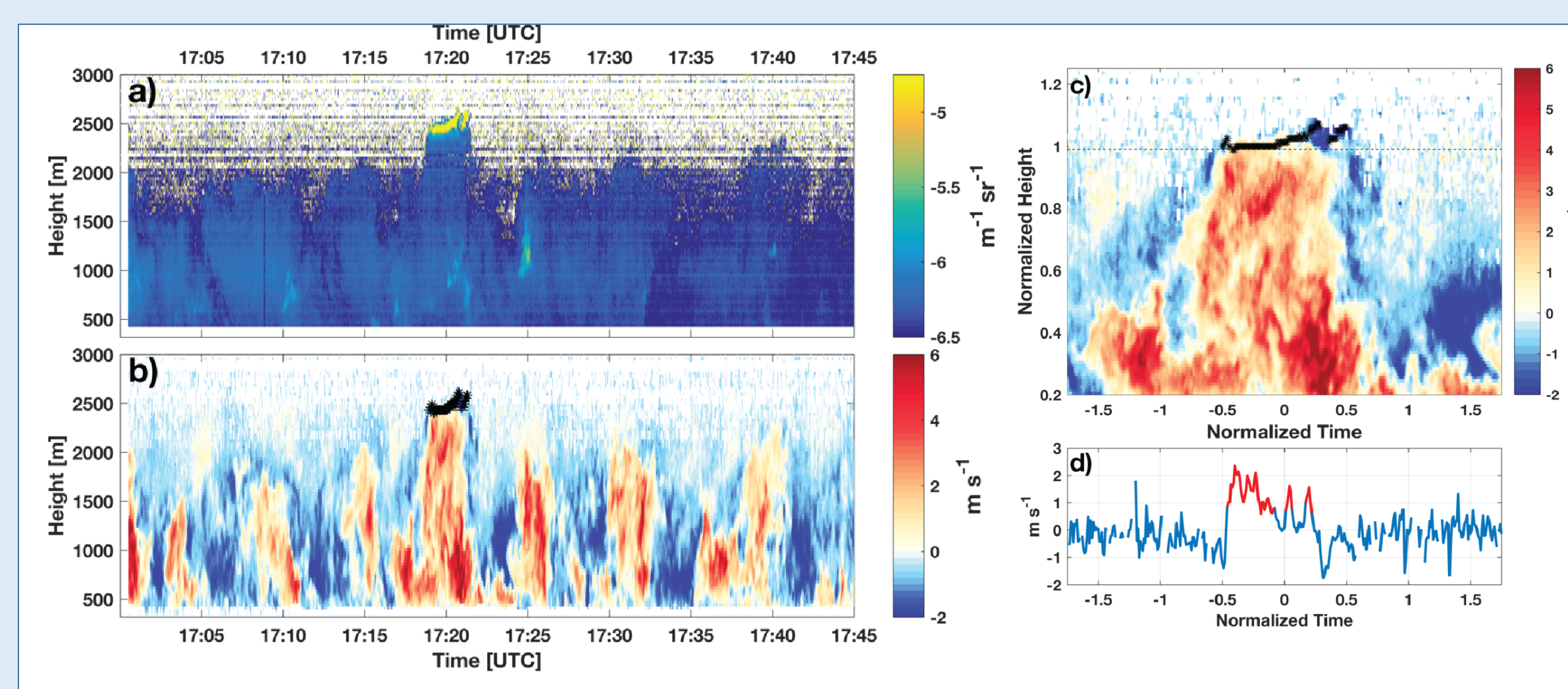
Fig. 5. Example of the cloud identification and subcloud circulation analysis. (a) Attenuated backscatter from the Doppler lidar showing the structure of the CBL and the presence of a single ShCu cloud (yellow shading). (b) DL vertical velocity (red/blue shading) and cloud base detections (black stars) for the same scene. (c) "Cloud scene" extracted from the lidar data wherein height is normalized by cloud base and time by cloud duration. (d) Cloud base vertical velocity determined 30 m below the cloud base. The red line segments indicate updrafts.

Fig. 6. Distribution of total cloud base mass flux across all 1495 shallow cumulus clouds.
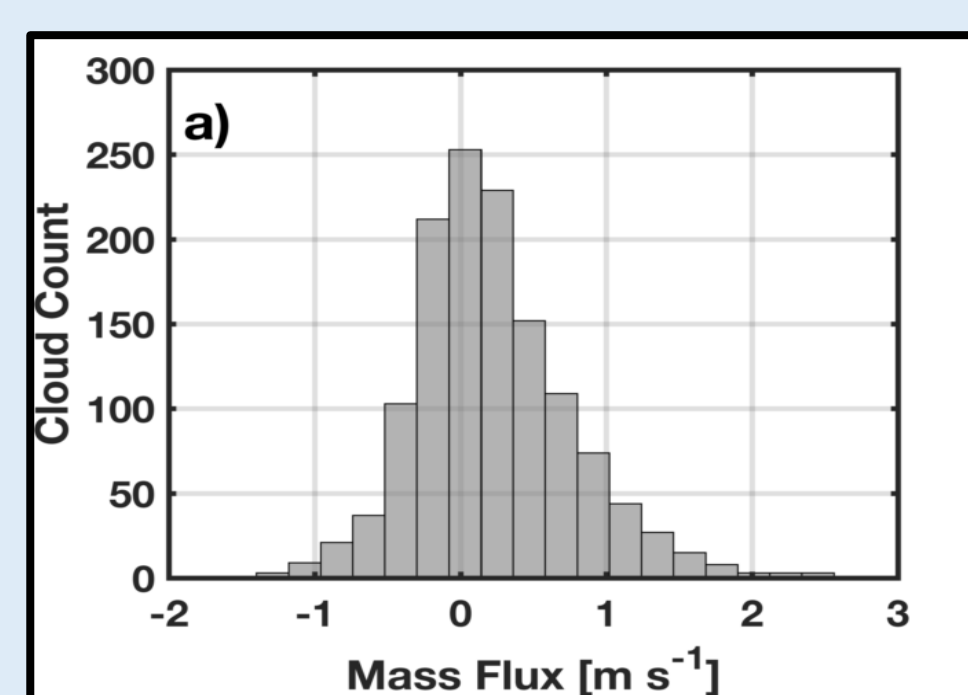
4. Composite subcloud circulation

The composite subcloud circulations for net positive and net negative mass flux clouds are shown in Fig. 7.

Positive mass flux clouds are associated with a coherent subcloud updraft extending over the depth of the CBL and extending into the cloud base. The updraft is slightly asymmetric in time, indicating a down wind tilt. The updraft is flanked by broad, weak downdrafts except near the cloud edges where a more concentrated downdraft occurs.

In contrast, the composite negative mass flux clouds are not associated with a coherent updraft, but still retain the compact downdrafts extending from the cloud edges. The origin of these flanking downdrafts remains a topic of investigation.
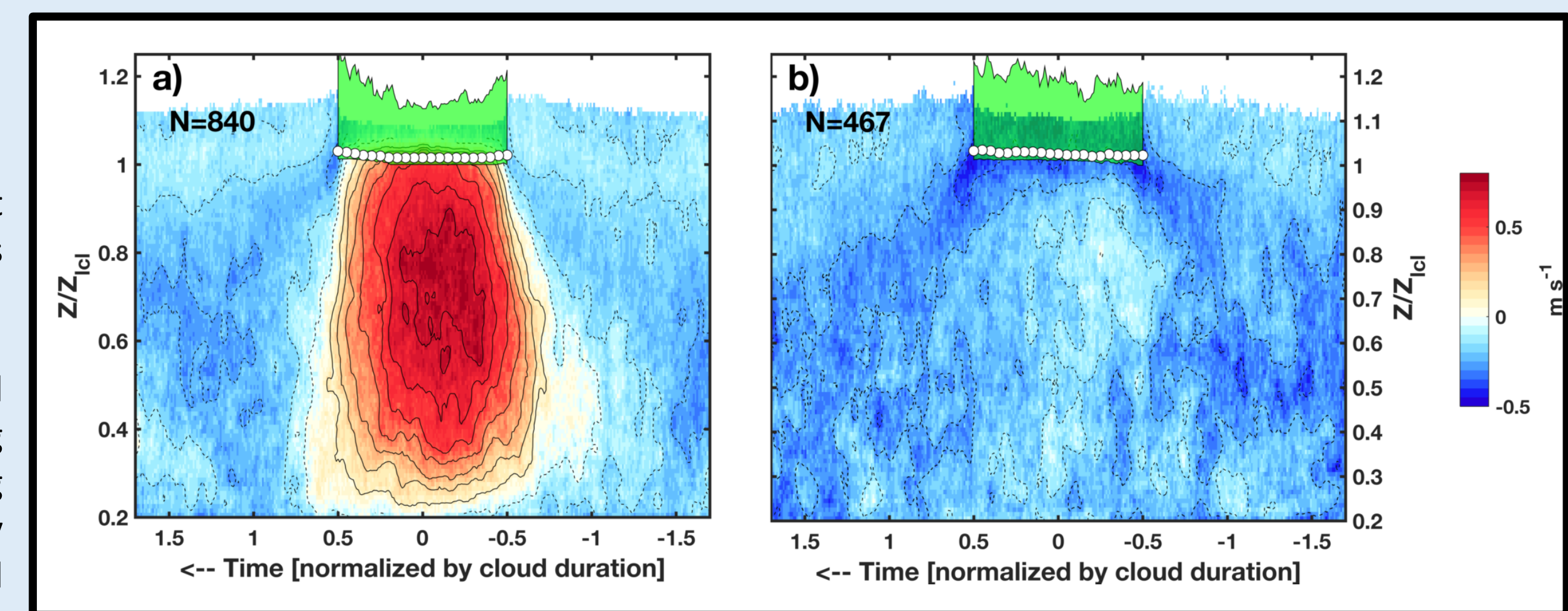
Fig. 7. Composite subcloud vertical velocity analysis for (a) positive mass flux clouds, and (b) negative mass flux clouds. The height is normalized by cloud base height and the time is normalized by cloud duration. Time increases to the left. The mean cloud base is indicated in white circles. The 95th percentile of cloud base height is shown in green.

5. CIN-Based Closure

The relationships amongst vertical velocity, stratification, and cloud development are examined by binning observations into 30-minute periods. Each period is characterized in terms of a total updraft fraction (fraction of the 30 minutes with active updrafts), updraft strength, and mean "energy barrier" value.

The "energy barrier" is a measure of the energy required for updrafts to penetrate to the LCL. Here we quantify this value in two ways:

(1) Computing the convective inhibition (CIN) for boundary layer parcels using the 1730 UTC radiosonde, which is near the time of cloud initiation.
(2) Using AERI potential temperature profiles to determine the mean Brunt-Vaisala Frequency (N) across the distance (H) separating the CBL top and the LCL

The strength of the energy barrier is then compared with the strength of cloud base updrafts (W_{cb}) during the sampling period to form dimensionless cloud control parameters:

$$Cloud\ Control\ 1 = \frac{NH}{W_{cb}}$$

$$Cloud\ Control\ 2 = \frac{\sqrt{CIN}}{W_{cb}}$$
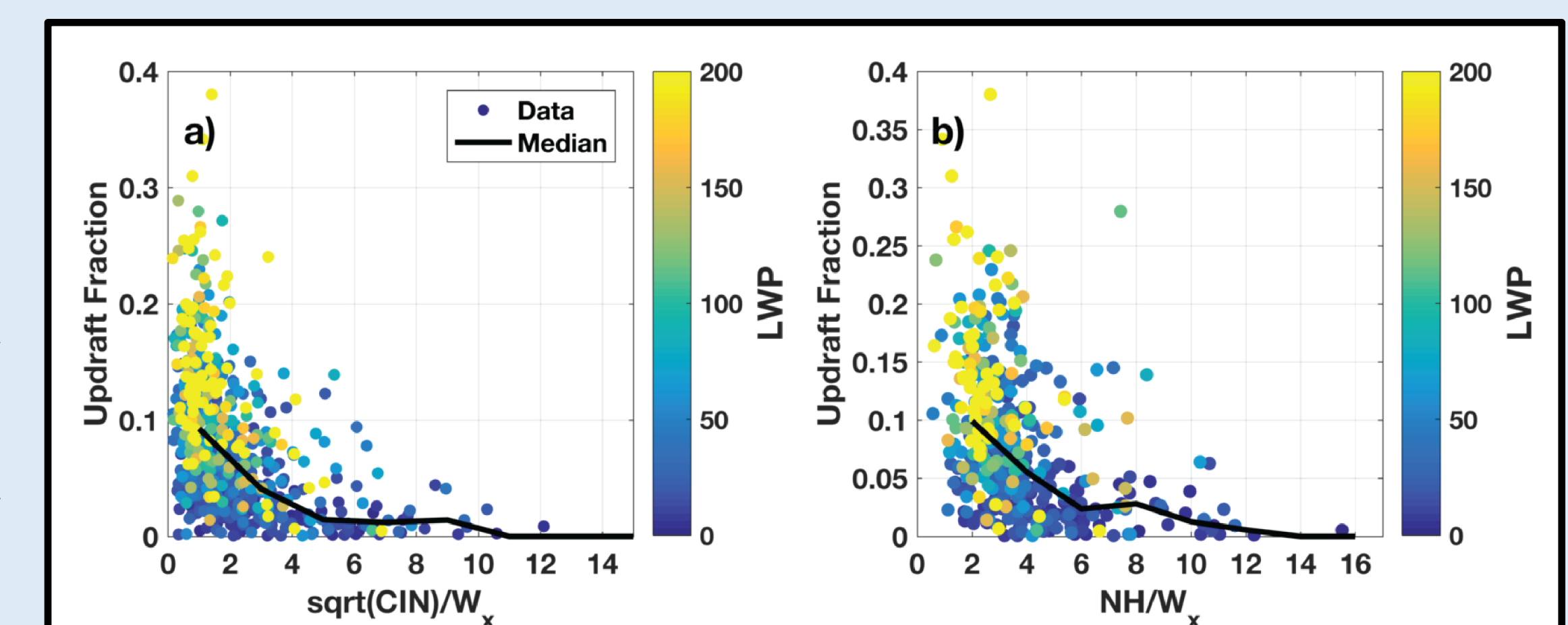
Fig. 8. Relationship between the hourly updraft fraction (ordinate) and the two dimensionless "cloud control" variables (abscissa). (a) Cloud control determined as the $\sqrt{CIN}/W_x$ and (b) cloud control determined as NH/W_x. In both panels the dots represent sample averaged data and the color fill is the 95th percentile of the LWP, as determined from the MWRP. The solid black line is the bin-median value. There are fewer available days with valid NH/W_x data, thus the more limited number of points.

In general, it is expected that when the updrafts (denominator) become strong relative to the energy barrier (numerator) that the updraft fraction, and thus the mass flux, will increase (Bretherton et al. 2004; Park and Bretherton 2009).

The observed relationship between updraft fraction and the two cloud control variables is shown in Fig. 8. Despite substantial scatter in the data, both analyses reveal the same functional relationship: the updraft fraction decays exponentially with increasing cloud control parameter. This finding is consistent with the expected relationship as well as LES studies (Fletcher and Bretherton 2012). Interestingly there is also a similar relationship between the cloud LWP and the cloud control variables.

6. Discussion

ShCU days are categorized by median cloud control value and then grouped by cloud control quartiles. Figure 9 shows the composite CBL evolution for each quartile. The time of cloud initiation is progressively later for increasing values of cloud control. Likewise, the cloud fraction is much higher (lower) on days with low (high) cloud control and, not surprisingly, the CBL must also grow deeper on high cloud control days in order to initiate clouds.

The surface forcing for CBL growth also varies across the quartiles. For the 2nd-4th quartiles the evaporative fraction (EF) progressively diminishes. Interestingly, the EF is lower in the first category than in the second suggesting the impact of ambient RH on cloud evolution.

In fact, boundary layer humidity substantively varies across the quartile composites. The highest (lowest) relative humidity corresponds with the lowest (highest) cloud control values (compare Figs. 10a-d). So too, the vertical gradient in the mixing ratio at the CBL top increases with increasing cloud control (compare Figs. 10e-h).
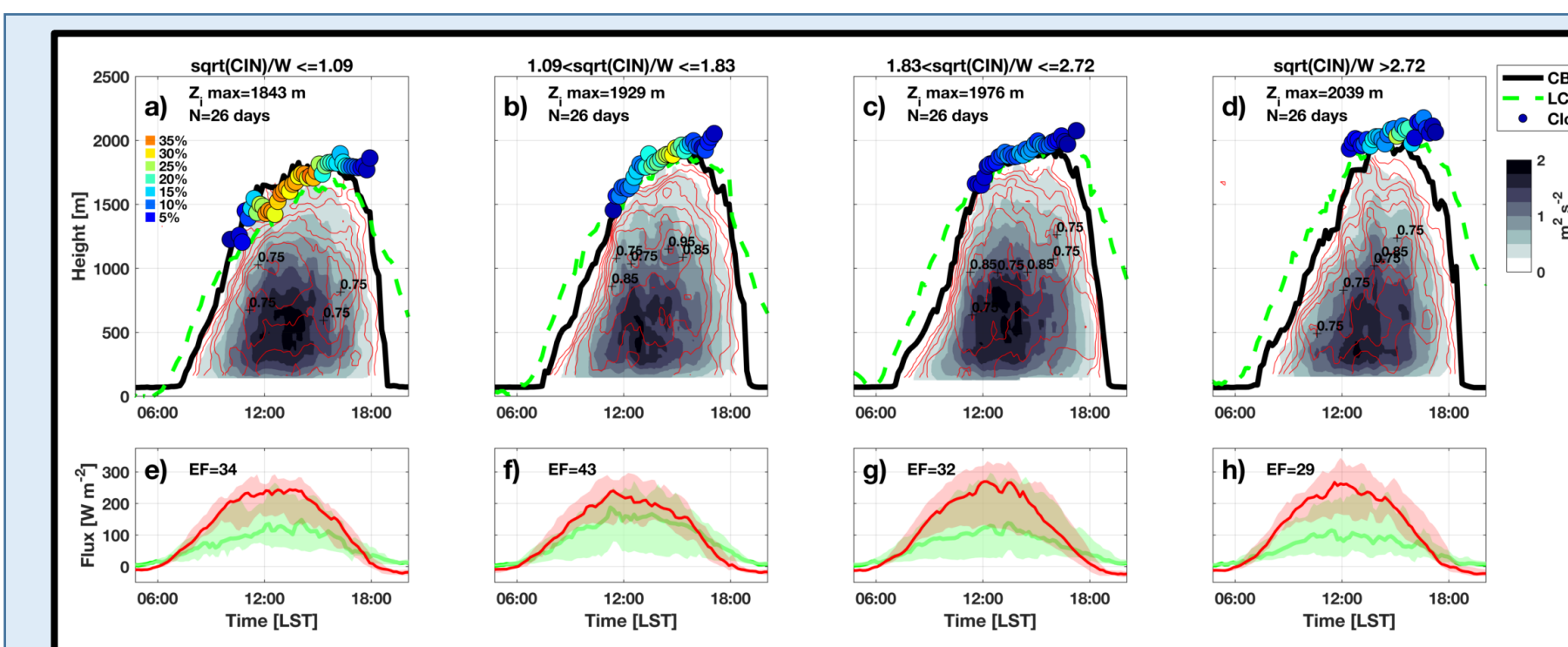
Fig. 9. CBL composites and surface forcing stratified by quartiles of the daily mean CIN based cloud control parameter. (a-d) CBL variables as in Fig. 2. (e-h) Surface fluxes and quartile ranges as well as the mean evaporative fraction (EF).
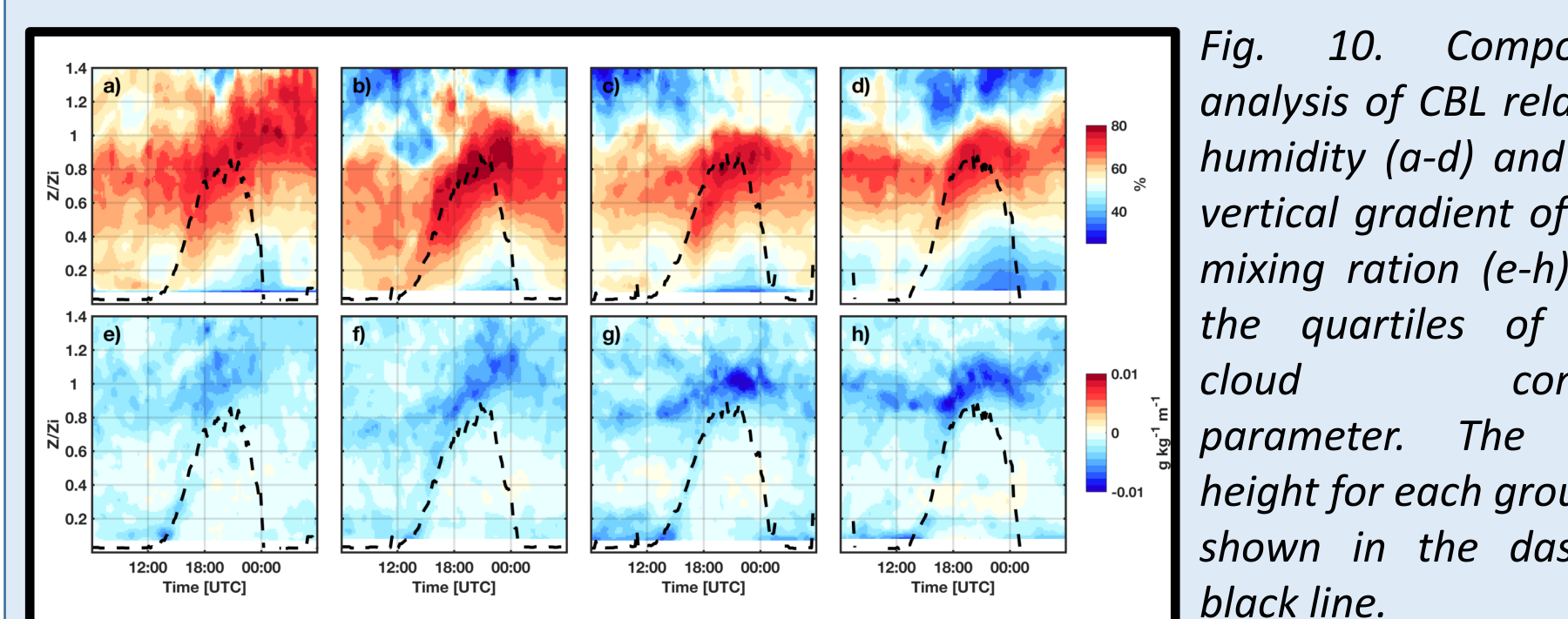
Fig. 10. Composite analysis of CBL relative humidity (a-d) and the vertical gradient of the mixing ratio (e-h) for the quartiles of the cloud control parameter. The CBL height for each group is shown in the dashed black line.

7. Summary and Conclusions

A suite of high resolution active remote sensors at ARM-SGP elucidate the links between CBL and cloud layer processes on days with ShCu. In addition to demonstrating the mean CBL properties these data reveal the relationship between sub-cloud updrafts and cloud layer stratification. Specifically, a dimensionless cloud control variable is shown to explain much of the observed variation in updraft fraction. This finding supports aspects of CIN-based closures for shallow convection. The dimensionless cloud control variable also captures dynamic and thermodynamic difference between days with varying degrees of shallow cumulus cloud cover.
For questions about this work please contact: neil.lareau@sjsu.edu

References

Bretherton, Christopher S., James R. McCaa, and Hervé Grenier. "A new parameterization for shallow cumulus convection and its application to marine subtropical cloud-topped boundary layers. Part I: Description and 1D results." Monthly Weather Review 132, no. 4 (2004): 864-882.

Fletcher, Jennifer K., and Christopher S. Bretherton. "Evaluating boundary layer-based mass flux closures using cloud-resolving model simulations of deep convection." Journal of the Atmospheric Sciences 67, no. 7 (2010): 2212-2225.

Park, Sungsu, and Christopher S. Bretherton. "The University of Washington shallow convection and moist turbulence schemes and their impact on climate simulations with the Community Atmosphere Model." Journal of Climate 22, no. 12 (2009): 3449-3469